References and Notes

1. M. D. Zoback *et al.*, *Science* **238**, 1105 (1987); V. S. Mount and J. Suppe, *J. Geophys. Res.* **97**, 11995 (1992); G. J. Axen, *ibid.* p. 8979; M. E. Magee and M. D. Zoback, *Geology* **21**, 809 (1993); A. H. Lachenbruch and G. A. Thompson, *Earth Planet. Sci. Lett.* **15**, 116 (1972); J. N. Brune, T. L. Henyey, R. F. Roy, *J. Geophys. Res.* **74**, 3821 (1969); A. H. Lachenbruch and J. H. Sass, *ibid.* **97**, 4995 (1992).
2. M. K. Hubbert and W. W. Rubey, *Bull. Geol. Soc. Am.* **70**, 115 (1959).
3. J. D. Byerlee, *Pure Appl. Geophys.* **116**, 615 (1978).
4. D. E. Moore, D. A. Lockner, R. Summers, S. Ma, J. D. Byerlee, *Geology* **24**, 1041 (1996); C. Morrow, B. Radney, J. Byerlee, in *Fault Mechanics and Transport Properties of Rock*, B. Evans and T.-F. Wong, Eds. (Academic Press, San Diego, CA, 1992), pp. 69–88. Brucite is a current possibility [D. E. Moore, K. Iwata, H. Tanaka, D. A. Lockner, J. D. Byerlee, *Eos Trans. AGU* **78**, F732 (1997).]
5. T. H. Heaton, *Phys. Earth Planet. Inter.* **64**, 1 (1990).
6. Equivalent to typical earthquake stress drops of 3 to 10 MPa [H. Kanamori and D. L. Anderson, *Bull. Seismol. Soc. Am.* **65**, 1073 (1975)].
7. Estimated with the results of L. J. Sonder [*Tectonics* **9**, 769 (1990)] and modified slightly for shear stress anomalies.
8. M. D. Zoback *et al.*, *Nature* **365**, 633 (1993).
9. Assuming hydrostatic fluid pressure, lithostatic average stress and a coefficient of friction of 0.6, the deviatoric stress when the optimally oriented plane is at failure is one-third of lithostatic. Over seismogenic depths (0 to 12 km) the average lithostatic stress is ~150 MPa.
10. J. R. Rice, in *Fault Mechanics and Transport Properties of Rock*, B. Evans and T.-F. Wong, Eds. (Academic Press, San Diego, CA, 1992), pp. 475–503.
11. J. Byerlee, *Geophys. Res. Lett.* **17**, 2109 (1990).
12. The San Bernardino segment results disagree with left-lateral stress orientations measured to 3.5-km depth in the Cajon Pass borehole, ~5 km northeast of the SAF [M. D. Zoback and J. H. Healy, *J. Geophys. Res.* **97**, 5039 (1992); G. Shamir and M. D. Zoback, *ibid.* p. 5059]. However, shear-wave anisotropy observed at Cajon Pass [Y. Liu, S. Crampin, R. E. Abercrombie, *Geophys. J. Int.* **129**, 439 (1997)] implies that, although the shallow stress orientation is as observed in the borehole, σ_H at seismogenic depths is ~45° to the fault in a right-lateral sense.
13. M. Wyss and Z. Lu, *Geophys. Res. Lett.* **22**, 547 (1995); L. M. Jones, *J. Geophys. Res.* **93**, 8869 (1988).
14. H. Magistrale and C. Sanders, *J. Geophys. Res.* **101**, 3031 (1996); L. Seeber and J. G. Armbruster, *ibid.* **100**, 8285 (1995).
15. J. W. Gephart and D. W. Forsyth, *ibid.* **89**, 9305 (1984).
16. Using the far-field orientation of σ_H relative to the fault, the shear and normal stress on fault-parallel planes is found, assuming that the average stress is lithostatic, the pore pressure is hydrostatic, and the optimally oriented plane is at failure stress. The shear and normal stress on fault-parallel planes, assumed to be uniform, is used to find the pore pressure needed for the fault to fail under a Coulomb failure criterion with a coefficient of friction of 0.6.
17. F. M. Chester, J. P. Evans, R. L. Biegel, *J. Geophys. Res.* **98**, 771 (1993).
18. M. L. Blanpied, D. A. Lockner, J. D. Byerlee, *Nature* **358**, 574 (1992).
19. R. H. Sibson, *Tectonophysics* **211**, 283 (1992); J. Byerlee, *Geology* **21**, 303 (1993); N. H. Sleep and M. L. Blanpied, *Nature* **359**, 687 (1992).
20. C. A. Morrow and J. D. Byerlee, *J. Geophys. Res.* **97**, 5145 (1992).
21. M. Lisowski, J. C. Savage, W. H. Prescott, *ibid.* **96**, 8369 (1991).
22. K. E. Sieh, *Bull. Seismol. Soc. Am.* **68**, 1731 (1978).
23. W. Thatcher, in *The San Andreas Fault System, California: U.S. Geol. Surv. Prof. Paper 1515*, R. E. Wallace, Ed. (Government Printing Office, Washington, DC, 1990), pp. 189–205.
24. M. J. Unsworth, P. E. Malin, G. D. Egbert, J. R. Booker, *Geology* **25**, 359 (1997); T. Yukutake, *Earthquake Predict. Res.* **3**, 345 (1985); S. Handa and N. Sumitomo, *J.* *Geomag. Geoelectr.* **37**, 93 (1985); C. Thurber *et al.*, *Geophys. Res. Lett.* **24**, 1591 (1997); D. Zhao, H. Kanamori, H. Negishi, D. Wiens, *Science* **274**, 1891 (1996); D. Zhao and H. Negishi, *J. Geophys. Res.* **103**, 9967 (1998); G. S. Fuis *et al.*, *Eos Trans. AGU* **77**, 173 (1996); T. A. Stern and J. H. McBride, *Tectonophysics* **286**, 63 (1998).
25. R. F. Yerkes, P. Levine, C. M. Wentworth, *U.S. Geol. Surv. Prof. Paper 1487*, M. J. Rymer and W. L. Ellsworth, Eds. (Government Printing Office, Washington, DC, 1990), p. 235; F. A. F. Berry, *Am. Assoc. Pet. Geol. Bull.* **57**, 1219 (1973).
26. D. A. Lockner and J. D. Byerlee, *Pure Appl. Geophys.* **145**, 717 (1995).
27. E. Hauksson, unpublished data.
28. A. J. Michael, *J. Geophys. Res.* **92**, 357 (1987).
29. Other fluctuations in the observed stress orientations may be due to major earthquakes [D. A. Castillo and M. D. Zoback, *ibid.* **100**, 6249 (1995); E. Hauksson, *Bull. Seismol. Soc. Am.* **84**, 917 (1994)] or topography and density anomalies [L. J. Sonder, *Tectonics* **9**, 769 (1990)].
30. Supported by the Southern California Earthquake Center (SCEC), NSF Cooperative Agreement EAR-8920136, U.S. Geological Survey (USGS) Cooperative Agreements 14-08-0001-A0899 and 1434-HQ-97AG01718, and USGS grant 99HQGR0039. We thank H. Kanamori, L. M. Jones, J. Deng, M. D. Zoback, and S. Hickman for valuable reviews and A. J. Michael and J. W. Gephart for sharing their stress inversion programs. This is SCEC contribution 452 and Caltech DGPS contribution 8586.

18 November 1998; accepted 7 June 1999

Estimation of Particulate Organic Carbon in the Ocean from Satellite Remote Sensing

Dariusz Stramski,[1]* **Rick A. Reynolds,**[1] **Mati Kahru,**[2] **B. Greg Mitchell**[2]

Measurements from the Southern Ocean show that particulate organic carbon (POC) concentration is well correlated with the optical backscattering by particles suspended in seawater. This relation, in conjunction with retrieval of the backscattering coefficient from remote-sensing reflectance, provides an algorithm for estimating surface POC from satellite data of ocean color. Satellite imagery from SeaWiFS reveals the seasonal progression of POC, with a zonal band of elevated POC concentrations in December coinciding with the Antarctic Polar Front Zone. At that time, the POC pool within the top 100 meters of the entire Southern Ocean south of 40°S exceeded 0.8 gigatons.

The phenomenon of POC sinking from the surface ocean is part of the biological pump, which provides a mechanism for sequestration of carbon in the deep ocean (*1*), but it has been difficult to estimate the amount and distribution of POC at basin and global scales from ship-based surveys. Here, we show that POC can be estimated from satellites and use this approach to analyze POC dynamics in the Southern Ocean. Our approach is based on two relations: first, the dependence of the backscattering coefficient by particles suspended in seawater, $b_{bp}(\lambda)$, on the POC concentration, and second, the dependence of the spectral remote-sensing reflectance, $R_{rs}(\lambda)$, on the total backscattering coefficient of seawater, $b_b(\lambda)$ (*2*). Note that $b_b(\lambda) = b_{bw}(\lambda) + b_{bp}(\lambda)$, where $b_{bw}(\lambda)$ is a constant representing the backscattering coefficient of pure seawater and λ is light wavelength (expressed in nanometers).

To derive an algorithm, we collected data during two cruises of the U.S. Joint Global Ocean Flux Study (JGOFS) within the Ant-

arctic Polar Front Zone (APFZ) along 170°W (between 50°S and 72°S) from January through March 1998, and one cruise within the Ross Sea in November and December 1997 along 76°30′S (169°E–178°W). The reflectance $R_{rs}(\lambda)$, defined as the ratio of upwelling radiance to downwelling irradiance just above the sea surface (*3*), was calculated from the underwater vertical profiles of downwelling irradiance and upwelling radiance measured with a MER-2040 spectroradiometer (*4*) (Biospherical Instruments, San Diego, California). The backscattering coefficient $b_b(\lambda)$ was obtained from measurements with a Hydroscat-6 sensor (*5*) (HOBI Labs, Watsonville, California), and the POC concentration was determined from the standard dry combustion analysis of samples that were taken with the ship's CTD (conductivity/temperature/depth)-rosette shortly before or after the optical casts. For the development of the satellite algorithm, only POC and $b_b(\lambda)$ measured within the top 15 m were used (typically from a depth of ~5 m).

POC and $b_{bp}(510)$ are highly correlated in both the APFZ and the Ross Sea, but the relation differs between the two regions (Fig. 1). The high correlation is caused by the dominance of the organic particle concentration in controlling changes in both POC and

[1]Marine Physical Laboratory and [2]Marine Research Division, Scripps Institution of Oceanography, University of California–San Diego, La Jolla, CA 92093–0238, USA.

*To whom correspondence should be addressed. E-mail: stramski@mpl.ucsd.edu

b_{bp} (6). Because the composition of particulate matter in a water body varies with time and from one location to another, some variability can be expected in the relation of POC versus b_{bp} (7). Our data show that particulate assemblages in the Ross Sea tend to backscatter less light than in the APFZ, especially at moderate to high POC concentrations. This difference may indicate that phytoplankton cells, whose contribution to b_{bp} is generally small (8), have a comparatively higher contribution to POC concentration in the Ross Sea. Part of the Ross Sea data was acquired
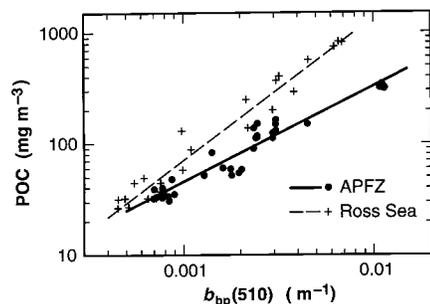

Fig. 1. Relationship between POC concentration and the particulate backscattering coefficient b_{bp} at 510 nm obtained from near-surface measurements in the APFZ and the Ross Sea. The fitted equation (solid line) for the APFZ is POC = $17069.0(\pm 1.3) \cdot [b_{bp}(510)^{0.859(\pm 0.046)}$ (r^2 = 0.918, n = 33)], while the corresponding equation (dashed line) for the Ross Sea is POC = $476935.8(\pm 1.5) \cdot [b_{bp}(510)^{1.277(\pm 0.061)}$ (r^2 = 0.953, n = 24)]. The standard errors of the estimates of the regression coefficients are given in parentheses, r^2 is the squared correlation coefficient (in this particular case, for the log-transformed variables), and n is the number of observations. The difference between the two relations indicates that site-specific algorithms may be necessary to ensure best possible estimates of POC from b_{bp} at regional scales.
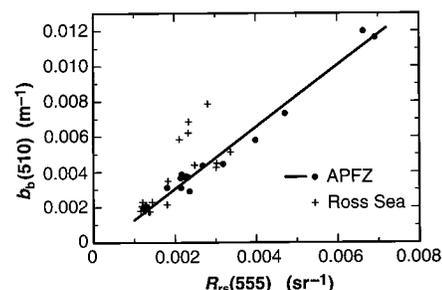

Fig. 2. Relationship between the total backscattering coefficient b_b at 510 nm and remote-sensing reflectance R_{rs} at 555 nm. Data from the APFZ are described by the fitted equation (solid line): $b_b(510)$ = $1.756(\pm 0.085) \cdot R_{rs}(555) - 4.772 \cdot 10^{-4} (\pm 3.106 \cdot 10^{-4})$ (r^2 = 0.972, n = 14). Data from the Ross Sea are consistent with the APFZ relation, with the exception of four measurements made within a bloom of *Phaeocystis antarctica*. These measurements were made at very high concentration of POC (566 to 822 mg m^{-3}), whereas all other measurements in both regions occurred at POC < 400 mg m^{-3}.

during an intense bloom of the Prymnesiophyte *Phaeocystis antarctica* (surface chlorophyll *a* as high as 14 mg m^{-3}), which supports this hypothesis. Regardless of variability, the data in Fig. 1 demonstrate the feasibility of establishing regional relations for estimating POC from b_{bp} with accuracy comparable to or better than the estimation of chlorophyll *a* from bio-optical models (9).

The remote-sensing reflectance $R_{rs}(\lambda)$ is dominated by the ratio of backscattering $b_b(\lambda)$ to absorption $a(\lambda)$ coefficients of seawater (2). Models are available for retrieving $a(\lambda)$ and $b_b(\lambda)$ from $R_{rs}(\lambda)$ (10, 11). However, no backscattering measurements were used in the development of these models, and

no rigorous validation of backscattering retrieval has been done. We applied a simple empirical approach to estimate b_b from R_{rs} based on our data, which show very high correlation between simultaneously measured $b_b(510)$ and $R_{rs}(555)$ (Fig. 2). We used R_{rs} at 555 nm because it is a SeaWiFS [Sea-viewing Wide Field-of-view Sensor (12)] band and, in most oceanic waters, variations in absorption by particles and dissolved substances at 555 nm have comparatively small effect on R_{rs}. Furthermore, this SeaWiFS band consistently shows good agreement between satellite-derived and in situ–measured values of R_{rs}. Our Hydroscat-6 instrument did not include the 555-nm band, so we used
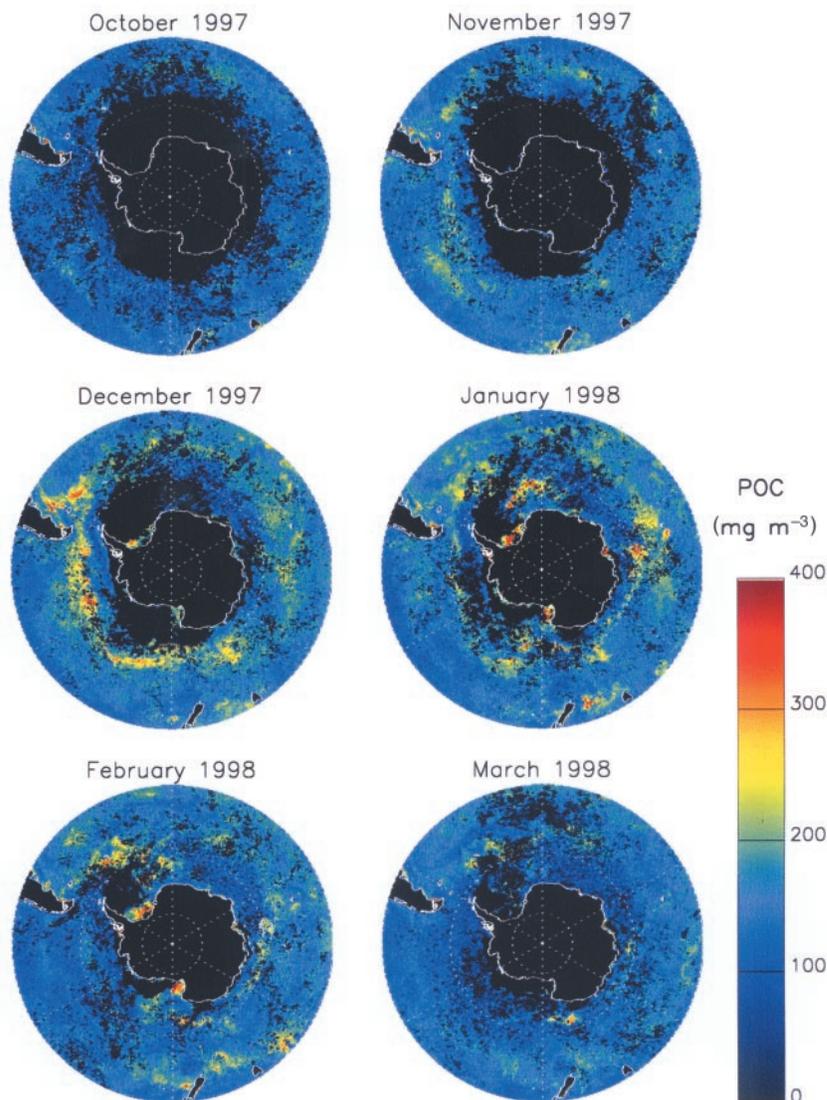

Fig. 3. The seasonal progression of POC concentration in the near-surface Southern Ocean all around Antarctica as determined from ocean color data collected by SeaWiFS. Monthly maps of POC from October 1997 through March 1998 were obtained by applying our algorithm to SeaWiFS monthly images of $R_{rs}(555)$ provided by NASA. Areas in black coincide with sea ice cover, cloudy skies, or both. The continental masses are also in black. Because our algorithm was developed using the APFZ data, the estimates of POC in coastal waters, polynyas, and marginal ice zones may be subject to larger uncertainties than in open ocean, as suggested by our results from the Ross Sea (see Fig. 1 and *Phaeocystis* bloom data in Fig. 2).

$b_b(510)$, which showed high correlation with both $R_{rs}(555)$ and POC, and thus proved to be adequate for our purposes. In contrast to POC versus $b_{bp}(510)$, the relation of $b_b(510)$ versus $R_{rs}(555)$ shows no significant difference between the two investigated regions, if four outlying data points collected in the Ross Sea during a bloom of *Phaeocystis* are excluded. This observation suggests that the backscattering and absorption coefficients in the 510- to 555-nm spectral region were well correlated over a wide range of particle concentrations and compositions.

By combining the relations of POC versus $b_{bp}(510)$ and $b_b(510)$ versus $R_{rs}(555)$ for the APFZ, we obtained the final algorithm for estimating POC (in milligrams per cubic meter) from $R_{rs}(555)$ (per steradian): POC = $17069[1.756 \cdot R_{rs}(555) - 1.777 \cdot 10^{-3}]^{0.859}$ (*13*). In this derivation, a value of 0.0013 m^{-1} was taken for backscattering by pure seawater, $b_{bw}(510)$ (*3*). We assume that the parameterization of our algorithm is valid for the Southern Ocean between 40°S and the marginal ice zone that the JGOFS study in the APFZ was intended to characterize. Strong mesoscale variability of the upper ocean properties and persistent cloud cover during our cruises prevented us from obtaining a large number of coincident in situ and satellite observations for validation purposes. Two measurements of surface POC were obtained under clear skies and ice-free water close in time to a SeaWiFS overpass. For these measurements, in situ values agreed to −8% and +2% with the satellite-derived values of POC for the pixels where the ship was located (*14*).

Application of our algorithm to SeaWiFS-derived $R_{rs}(555)$ reveals the progression of surface POC concentration in the Southern Ocean during the austral spring and summer from October 1997 through March 1998 (Fig. 3). In October, the large extent of seasonal ice is evident, and POC values were low throughout the ice-free Southern Ocean. By December, sea ice retreated and a band of elevated POC (>200 mg m^{-3}) developed nearly all around Antarctica. This band corresponds to the average position of the APFZ (*15*). In the Pacific sector, a well-pronounced band of high POC followed the 60°S latitude in the southeast and extended north of 60°S over the Pacific-Antarctic Ridge, which coincides well with the APFZ. In the Atlantic and Indian Ocean sectors, the band of enhanced POC, although less pronounced, was shifted farther north, which again is consistent with the APFZ pattern. The high POC feature north of the Falkland Islands also agrees with the northward extension of the APFZ observed in this region (*15*). Starting in January, areas of high POC became progressively smaller, and by March, the surface POC was <150 mg m^{-3} over most of the Southern Ocean.

Many of the POC features are similar to the seasonal progression of phytoplankton biomass.

The SeaWiFS-derived images of chlorophyll a (Chl) for the same season show generally low pigment concentrations in the early season, a development of blooms in December and January, followed by a sharp decline in Chl in March (*16*). The various phytoplankton blooms (or high Chl areas), for example within the APFZ of the Pacific sector, over the Patagonian Shelf, in the Scotia Sea, and near Kerguelen, are coincident with the high POC regions and show progression throughout the season that is similar to that of POC. However, the POC:Chl ratio in the upper ocean varies considerably because of varying proportions of nonliving organic particles, phytoplankton, and heterotrophic microorganisms. This ratio varied from 112 to 455 during our two cruises in the APFZ. This variability precludes the estimation of POC from satellite-derived Chl with reasonable accuracy.

The surface POC concentration is correlated with the mass of POC integrated within the upper water column (*17*). By applying such a relation to the satellite-derived monthly maps of surface POC, we calculated the changes in the total mass of POC within the top 100 m in the Southern Ocean between 40°S and 70°S over the annual cycle from October 1997 through December 1998. These calculations excluded the austral winter (May through August), because extensive ice cover and lack of daylight over large portions of the Southern Ocean precluded satellite observations of ocean color. The total amount of water column–integrated POC ranges from about 0.6 Pg of carbon (1 Pg = 10^{15} g = 1 gigaton) in April 1998 and September 1998 to 0.8 Pg of carbon in December 1997 and December 1998. The two December estimates agree to within 0.9%. If we included the areas south of 70°S (that is, primarily polynyas within the Antarctic sea ice zone), the December estimates would increase to about 0.87 Pg of carbon (note however that south of 70°S, the number of valid satellite pixels decreases sharply due to sea ice, which may lead to less accurate estimates). In June and July, the POC pool is likely reduced to <0.5 Pg, which indicates that the net seasonal change between the summer maximum and winter minimum is >0.3 Pg of carbon.

References and Notes

1. R. W. Eppley and B. J. Peterson, *Nature* **282**, 677 (1979); T. Volk and M. I. Hoffert, *The Carbon Cycle and Atmospheric CO₂: Natural Variations Archean to Present*, E. T. Sundquist and W. S. Broecker, Eds. (*Geophys. Monogr.* vol. 32, American Geophysical Union, Washington, DC, 1985), pp. 99–110; A. R. Longhurst and W. G. Harrison, *Prog. Oceanogr.* **22**, 47 (1989).
2. H. R. Gordon, O. B. Brown, M. M. Jacobs, *Appl. Opt.* **14**, 417 (1975); A. Morel and L. Prieur, *Limnol. Oceanogr.* **22**, 709 (1977).
3. C. D. Mobley, *Light and Water: Radiative Transfer in Natural Waters* (Academic Press, San Diego, CA, 1994), pp. 60–144.
4. B. G. Mitchell and M. Kahru, *Calif. Coop. Oceanic Fish. Invest. Rep.* **39**, 133 (1998).
5. R. A. Maffione and D. R. Dana, *Appl. Opt.* **36**, 6057 (1997).
6. Although there is no previous data showing the relation between POC and b_{bp}, circumstantial evidence suggesting correlation between the two variables has been available. Data collected in different parts of the world's oceans indicate that particulate scattering (b_p) or beam attenuation (c_p) coefficients are correlated with POC [W. D. Gardner, I. D. Walsh, M. J. Richardson, *Deep-Sea Res. II* **40**, 171 (1993); J. Marra, C. Langdon, C. A. Knudson, *J. Geophys. Res.* **100**, 6633 (1995); H. Loisel and A. Morel, *Limnol. Oceanogr.* **43**, 847 (1998)]. Laboratory experiments with phytoplankton cultures showed similar correlations [D. Stramski and A. Morel, *Deep-Sea Res.* **37**, 245 (1990); D. Stramski and R. A. Reynolds, *Limnol. Oceanogr.* **38**, 1347 (1993)]. Because b_{bp}, b_p, and c_p are expected to be well correlated with one another (especially at light wavelengths where absorption is small), our results in Fig. 1 are qualitatively consistent with previous observations that involved b_p or c_p.
7. The variations in the particulate composition are accompanied by changes in particle size, shape, and refractive index distributions, which all influence b_{bp} [C. F. Bohren and D. R. Huffman, *Absorption and Scattering of Light by Small Particles* (Wiley, New York, 1983)]. However, carbon content in individual planktonic cells is coupled with particle size [P. G. Verity *et al.*, *Limnol. Oceanogr.* **37**, 1434 (1992); D. J. Montagnes *et al.*, *ibid.* **39**, 1044 (1994)] and refractive index [D. Stramski, *Deep-Sea Res.* **46**, 335 (1999)], which may reduce the variability in the relation of POC versus b_{bp} that is associated with changes in particle composition.
8. A. Morel and Y.-H. Ahn, *J. Mar. Res.* **49**, 177 (1991); D. Stramski and D. A. Kiefer, *Prog. Oceanogr.* **28**, 343 (1991).
9. The relative error of the order of 30 to 40% was reported for chlorophyll retrieval from empirical algorithms based on the ratio of upwelled radiances when applied to Coastal Zone Color Scanner data in Case 1 waters with pigment concentrations ranging from about 0.1 to 1.5 mg m^{-3} [H. R. Gordon *et al.*, *J. Mar. Res.* **40**, 491 (1982); H. R. Gordon *et al.*, *Appl. Opt.* **22**, 20 (1983)].
10. S. A. Garver and D. A. Siegel, *J. Geophys. Res.* **102**, 18607 (1997).
11. K. L. Carder *et al.*, *ibid.* **104**, 5403 (1999).
12. S. B. Hooker *et al.*, *NASA Tech. Memo. 104566*, vol. 1 (1992).
13. Our algorithm was obtained from two separate relations rather than a direct correlation between POC and $R_{rs}(555)$, because this two-step approach offers a sound conceptual framework for understanding the performance of the algorithm. The inherent optical property, b_{bp}, is linked to the concentration of a seawater constituent, POC, and the apparent optical property, R_{rs}, is linked to the inherent optical property, b_b (*18*). Furthermore, our data suggest that the relation of POC versus $b_{bp}(510)$ may be more sensitive to regional variations than the relation of $b_b(510)$ versus $R_{rs}(555)$. The two-step approach can also be useful for future refinements. For example, as more data from concurrent measurements of R_{rs} and b_b in the ocean become available, it may be advantageous to retrieve b_b from R_{rs} using semi-analytic multispectral algorithms similar to that described by Carder *et al.* (*11*) rather than a simple empirical relation.
14. Two in situ measurements were made in the Ross Sea on 1 December 1997 at the western end of the transect (76°30′S, 169°E) close in time to a SeaWiFS overpass (less than 5 hours difference). High-resolution picture transmission SeaWiFS data corresponding to these in situ observations were acquired by the McMurdo station, Antarctica. The satellite data were first processed to obtain $R_{rs}(555)$ averaged over 3 km by 3 km areas, and then POC was derived using our algorithm. In this particular case, the Ross Sea relation rather than the APFZ relation from Fig. 1 was used. The satellite-derived values of POC are 69.4 and 86.8 mg m^{-3}, which compare well with the actual measurements of POC, 75.7 and 85.0 mg m^{-3}, respectively.
15. M. Tomczak and J. S. Godfrey, *Regional Oceanography: An Introduction* (Pergamon, London, 1994), pp. 67–87.
16. K. Moore and M. Abbott, in *U.S. JGOFS Proceedings Report, AESOPS Data and Science Workshop #1* (U.S.

JGOFS Planning and Coordination Office, Woods Hole, MA, 1998), pp. 247–253.

17. Our in situ measurements of spectral downwelling irradiance in the APFZ indicated that the 0.1% level of surface irradiance at 490 nm is, on average, 94 m. To a first approximation, we assume the 100 m depth delimits the upper layer where most organic carbon production by photosynthesis occurs. From vertical profiles of POC concentration, we established the relation between the water column POC integrated from the surface to 100 m depth (in milligrams per square meter) and the surface concentration of POC (in milligrams per cubic meter), which is: POC (water column–integrated) = 53.36 ($\pm$3.83) · POC (surface concentration) + 2341.41 ($\pm$361.56). The standard errors of the regression coefficients are given in parentheses, the squared correlation coefficient is 0.894, and the number of observations is 25.

18. The inherent optical properties (IOPs) are those properties that depend only on the medium, and not on the geometric (directional) structure of the ambient light field within the medium. In the ocean, the IOPs (which include the backscattering coefficient b_b) depend on the concentration and composition of optically significant constituents of seawater. The apparent optical properties (AOPs) are those properties that depend both on the medium (the IOPs) and on the geometric structure of the ambient light field, and that display enough regular features and stability to be useful descriptors of the medium [R. W. Preisendorfer, *Union Geod. Geophys. Inst. Monogr.* **10**, 11 (1961); (*3*)].

19. We thank J. Wieland, B. Bichnevicius, the technical staff of Antarctic Support Associates, and the officers and crew of the R/V *Nathaniel B. Palmer* and R/V *Roger Revelle*. We also thank the SeaWiFS Project and the NASA Distributed Active Archive Center at the Goddard Space Flight Center for the production and distribution of the SeaWiFS data. This research was supported by NASA and NSF as part of the U.S. JGOFS Antarctic Environment Southern Ocean Process Study.

1 March 1999; accepted 8 June 1999

A Nucleoside Transporter from *Trypanosoma brucei* Involved in Drug Resistance

Pascal Mäser,[1]* Christine Sütterlin,[2]* Anastasia Kralli,[2] Ronald Kaminsky[1]†‡

Drug resistance of pathogens is an increasing problem whose underlying mechanisms are not fully understood. Cellular uptake of the major drugs against *Trypanosoma brucei* spp., the causative agents of sleeping sickness, is thought to occur through an unusual, so far unidentified adenosine transporter. *Saccharomyces cerevisiae* was used in a functional screen to clone a gene (*TbAT1*) from *Trypanosoma brucei brucei* that encodes a nucleoside transporter. When expressed in yeast, *TbAT1* enabled adenosine uptake and conferred susceptibility to melaminophenyl arsenicals. Drug-resistant trypanosomes harbor a defective *TbAT1* variant. The molecular identification of the entry route of trypanocides opens the way to approaches for diagnosis and treatment of drug-resistant sleeping sickness.

Reduced drug uptake has emerged as a common characteristic of drug-resistant trypanosomes [(*1*); reviewed in (*2*)], rendering the molecular identification of drug transport systems crucial for the understanding of the underlying resistance mechanisms. The main clinical trypanocides are the melaminophenyl arsenical melarsoprol and diamidines. As cellular uptake of these agents has been suggested to occur through a transport system specific for adenosine and adenine [(*3–5*); reviewed in (*6*)], we decided to functionally clone the trypanosomal gene or genes encoding an adenosine transporter or transporters. We took advantage of the fact that the yeast *Saccharomyces cerevisiae* do not take up exogenous adenosine and cannot use it as a purine source (Fig. 1, A and B). Yeast cells defective in purine biogenesis (*ade2*) (*7*) were transformed with a *Trypanosoma brucei brucei* bloodstream form cDNA expression library (*8*) and selected for growth in media containing adenosine as sole purine source. Library plasmids conferring the ability to proliferate were isolated (*9*) and found to encode a putative transporter, designated TbAT1. When expressed in yeast, *TbAT1* enabled growth on adenosine as sole purine source (Fig. 1A) and cellular uptake of adenosine (Fig. 1B). Adenosine transport was saturable (Fig. 1C) and conformed to Michaelis-Menten kinetics with an apparent Michaelis constant (K_m) of 2.2 μM (*10*).

Trypanosoma brucei brucei salvage adenosine from their mammalian hosts through two high-affinity transport activities, P1 and P2, that differ in substrate specificity. P1 is specific for adenosine and inosine, whereas P2 transports adenosine, adenine, melaminophenyl arsenicals, and diamidines (*3*, *4*). To determine whether *TbAT1* encodes the P1 or P2 activity, we assessed substrate specificity by the ability of potential substrates to inhibit TbAT1-mediated adenosine transport in yeast (*11*). Adenine caused a strong reduction, whereas inosine, hypoxanthine, guanosine, guanine, uridine, and uracil had no effect (Fig. 2A). Moreover, radioactively labeled inosine was not taken up, and neither inosine nor guanosine could support growth of *ade2* yeast expressing *TbAT1* (*12*). Among the trypanocides tested for inhibition of adenosine transport, the melaminophenyl arsenicals (melarsoprol and melarsen oxide) and isometamidium (a phenanthridine used in veterinary medicine) were most effective (Fig. 2B), suggesting that these drugs are TbAT1 substrates. The experimental compound tubercidin (7-deazaadenosine) produced a smaller but substantial reduction. The diamidines (pentamidine and diminazene aceturate) had no substantial effect. Thus, the apparent substrate specificity of TbAT1 closely matches that of the reported P2 transport activity (*3–5*), except for the insensitivity to diamidines. TbAT1 expressed in yeast may lack a trypanosomal cofactor or modification required for diamidine recognition. Future studies of TbAT1 function in genetically engineered trypanosomes will elucidate the role of this transporter in diamidine uptake.

As labeled melaminophenyl arsenicals are unavailable, we could not directly measure transport of these drugs by TbAT1. Instead, we determined whether TbAT1 could mediate uptake of melarsen oxide into cells, measured as susceptibility to the drug (*13*). Expression of *TbAT1* in yeast rendered cell growth sensitive to melarsen oxide (Fig. 2C), suggesting that TbAT1 indeed transports this drug. As expected for competing substrates, the presence of adenosine or adenine in the media abrogated TbAT1-mediated melarsen toxicity (*12*).

Sequencing of the cDNA revealed a protein of 463 amino acids (Fig. 3A) with a predicted structure of 10 transmembrane α-helices, cytosolic NH_3- and CO_2-termini, and a large, negatively charged cytosolic loop between transmembrane domains 6 and 7 (Fig. 3B). Recently, two nucleoside transporter genes (*LdNT1.1* and *LdNT1.2*) have been cloned from the protozoan parasite *Leishmania donovani* (*14*). *LdNT1.1* and *LdNT1.2* are 99.5% identical and tandemly linked (*14*, *15*). In contrast, *TbAT1* appears to be a single-copy gene, as determined by Southern (DNA) blot analysis (*12*). The LdNT1 transporters belong to the ENT (equilibrative nucleoside transporter) family, feature 11 predicted transmembrane domains,

[1]Swiss Tropical Institute, CH-4002 Basel, Switzerland. [2]Biozentrum, University of Basel, CH-4056 Basel, Switzerland.

*Present address: Department of Biology, University of California, San Diego, La Jolla, CA 92093, USA.
†Present address: Novartis CRA, CH-1566 St. Aubin, Switzerland.
‡To whom correspondence should be addressed. E-mail: ronald.kaminsky@ah.novartis.com